/lasmedigitalcollection.asme.org/mechanismsrobotics/article-pdf/15/1/04502/6880708/jmr_15_1_014502.pdf?casa_token=AxY9tgUQSasAAAA:cwBeFEF5MkPFHCpFEPn1uKi2XmBzJg6X4rcliCkPpiF0DZZ_R9mSk3M1nhBvtlnervAE8ng by Purdue University at West Lafayette user on

Feasibility Design and Control of a Lower Leg Gait Emulator Utilizing a Mobile 3-Revolute, Prismatic, Revolute Parallel Manipulator

Ahmed Soliman

Polytechnic Institute, Purdue University, 401 N Grant Street, West Lafayette, IN 47907 e-mail: solimana@purdue.edu

Guilherme A. Ribeiro

Polytechnic Institute, Purdue University, 401 N Grant Street, West Lafayette, IN 47907 e-mail: garamizo@purdue.edu

Dongming Gan

Polytechnic Institute, Purdue University, 401 N Grant Street, West Lafayette, IN 47907 e-mail: dgan@purdue.edu

Mo Rastgaar¹

Polytechnic Institute, Purdue University, 401 N Grant Street, West Lafayette, IN 47907 e-mail: rastgaar@purdue.edu

Design and control of lower extremity robotic prostheses are iterative tasks that would greatly benefit from testing platforms that would autonomously replicate realistic gait conditions. This paper presents the design of a novel mobile 3-degree-of-freedom (DOF) parallel manipulator integrated with a mobile base to emulate human gait for lower limb prosthesis evaluation in the sagittal plane. The integrated mobile base provides a wider workspace range of motion along the gait direction and reduces the requirement of the parallel manipulator's actuators and links. The parallel manipulator design is optimal to generate the defined gait trajectories with both motion and force requirements using commercially available linear actuators. An integrated active force control with proportional integral derivative (PID) control provided more desirable control compared to traditional PID control in terms of error reduction. The novelty of the work includes the methodology of human data-oriented optimal mechanism design and the concept of a mobile parallel robot to extend the translational workspace of the parallel manipulator with substantially reduced actuator requirements, allowing the evaluation of prostheses in instrumented walkways or integrated with instrumented treadmills. [DOI: 10.1115/1.4053825]

Keywords: mobile parallel manipulator, gait emulator, active force control, inverse kinematics, forward kinematics, bioinspired design, parallel platforms, prosthetics

1 Introduction

The design and development of powered and passive prostheses require extensive testing using human subjects. Test clearances, safety, and the lack of repeatability associated with human trials may be reduced with automated testing [1]. Gait experiments require a large amount of repetition in different types of gait maneuvers, taking long hours causing fatigue in human subjects that may influence the outcomes of the clinical trials. A gait emulator for testing lower extremity prostheses that can be used independently of a human subject may speed up the design and evaluation process and improve their readiness for clinical trials [2]. In recent years, studying the human gait has been extended to studying the neuromuscular characteristics of the human ankle during gait, including the ankle mechanical impedance. The Perturbation platforms, whether 1-degree-of-freedom (DOF) [3] or 2-DOF [4-6] that are installed in the instrumented walkways have been essential to these studies. A gait emulator that can reliably and repetitively replicate realistic gait cycles on an instrumented walkway equipped with these perturbation platforms can be beneficial to the iterative process of design and control of lower extremity robotic prostheses. Such an emulator can increase the efficiency for the fine-tuning of the controller gains, estimating error in achieving desired ankle impedance [5], and studying high-level controllers such as locomotion mode, and user intent control of the prosthesis. The significance of this design approach includes the capability of evaluating the lower limb prostheses' features on instrumented walkways without the need for a human subject, addressing one of the challenges of such studies is the need for extensive data set of gait cycles. This motivates our work to design and eventually build a mobile 3-RPR (revolute, actuated prismatic, revolute) parallel manipulator capable of emulating gait maneuvers of the human lower leg over instrumented walkaways [7].

Gait emulators have been widely used in the past for injury rehabilitation and prostheses evaluations. The majority of the gait emulators are stationary platforms that may be installed over treadmills that may or may not include human subjects for testing of the prostheses. Collins et al. [8] designed an ankle-foot prosthesis emulator that was connected to ampute subjects over a treadmill with control of Plantarflexion and inversion-eversion torque. Chiu et al. [9] assembled an ankle-foot prosthesis emulator capable of modulating the center of pressure of the prosthetic ankle while connected to an amputated subject. Yul Shin et al. [10] designed a gait emulator to help re-train people with neurological injuries. A single motor actuated an eight-link Jansen mechanism over a treadmill depending on the desired gait trajectory. Lee [11] implemented a stationary exoskeleton emulator system with offload torque actuation in the hip, knee, and ankle hip joints in the sagittal plane to estimate the hip joint impedance. Hedrick et al. [12] utilized an immobilizer boot with a robotic ankle-foot prosthesis emulator. The prosthesis emulator utilized healthy human subjects to test five ankle stiffness conditions, seeking to emulate the quasi-stiffness of a healthy human ankle using an ankle-foot prosthesis. Alamdari et al. [13] implemented a scaled planar elastic articulated-cable leg-orthosis emulator for human subject gait training. Thatte et al. [14] achieved lower limb prosthesis stance control via gait phase estimation, emulating human gait using a varying speed treadmill and a human subject. Azocar et al. [15] designed the open-source leg, a scalable robotic knee/ankle prosthesis intended to foster research in control strategies of powered lower limb prosthesis. The non-stationary gait emulator proposed in this paper allows researchers to observe the time-varying characteristics of a prosthetic ankle over an instrumented walkway, without the need for a human subject. In this paper, the design, simulation, and control of a novel mobile 3-RPR parallel manipulator with hybrid motion control are studied.

¹Corresponding author.

Contributed by the Mechanisms and Robotics Committee of ASME for publication in the JOURNAL OF MECHANISMS AND ROBOTICS. Manuscript received June 2, 2021; final manuscript received January 30, 2022; published online May 12, 2022. Assoc. Editor: Reza Fotouhi.

Parallel manipulators have an advantage over serial manipulators because they are known to have high stiffness capabilities, which allows rigidity against unwanted movements and disturbances [16]. Amirat et al. [17] developed a 6-DOF parallel manipulator to emulate equestrian paths to train users on various movements. Chen and Wang [18] proposed adding a mobile base to a lift assister, where a 3-revolute, actuated prismatic, and spherical manipulator sat on top of a remote-controlled cart. For the design of parallel manipulators, various extensive studies of kinematics, and singularity analysis are available. Inverse kinematics of parallel manipulators are straightforward relative to the serial manipulators and provide closed-form solutions. Alternatively, forward kinematics problems of parallel manipulators are more challenging to solve [16]. Lenarčič and Wenger [19] studied numerical solutions of the forward kinematics of various parallel manipulators, eliminating solutions through different singularity case analyses using path planning of various parallel manipulators. Using the Cayley formula and singularity loci, Gan et al. [20] investigated the forward kinematics of multiple parallel mechanisms. Gosselin and Angels [21] classified three different types of singularity configurations investigated through the Jacobian matrix. Joshi and Tsai [22] proposed the use of reciprocal screw theory to derive the Jacobian matrix to analyze singularity configurations. Kong studied Type II singularity free regions of 3-revolute, prismatic, revolute (RPR) manipulator using numerical analysis of the relationship between manipulator design and desired end-effector configuration [23].

In addition to the inherent complexity in the design of parallel manipulators, their control is also challenging [16]. Proportional integral derivative (PID) controller was used for a 6-DOF parallel manipulator to mimic equestrian trajectories [17]. Noshadi et al. compared the effect of controlling a 3-RRR (Revolute, Revolute, Revolute) parallel manipulator using PID control in conjunction with active force control (AFC) and showed it was more effective and robust than PID control alone [24]. Honegger et al. [25] worked on adaptive feedforward control of a 6-DOF parallel manipulator for use as a high-speed milling machine.

In this paper, the proposed mobile 3-RPR parallel manipulator design incorporates a moving base that allows for significant translation and an onboard parallel manipulator that generates a precise trajectory of the lower leg in the sagittal plane. An optimization technique was employed to minimize the force, velocity, and stroke requirements of the actuated joints. Traditional PID control integrated with AFC was implemented in the optimized 3-RPR parallel manipulator to follow the desired human gait trajectories. Gradient descent optimization technique was used to solve the forward kinematics problem of the 3-RPR parallel manipulator. MATLAB and

Simulink were used to simulate the dynamics of the designed parallel manipulator.

2 Desired Trajectories

Six able-bodied subjects (21 to 45 with an average of $28.67 \pm$ 7.82 years old) with no self-reported history of neuromusculoskeletal pathology or ankle impairment participated in gait experiments to define the trajectory design requirements for the mobile 3-RPR parallel manipulator. All subjects gave written content to participate in the experiment, as approved by the Institutional Review Board (application numbers 423498-10, 371107-9, and 371102-8). A motion capture camera system (Miqus M5, Qualisys) and a force plate (9260AA3, Kistler, Switzerland) recorded the individual shank trajectory, and the ground reaction forces and torques during the gait cycle, respectively as subjects walked on a walkway [5]. The recorded trajectory of the human shank contains information of its translation and rotation in six DOF, during a complete gait cycle. Straight walk gait cycles are represented by three of the six DOFs, namely the translation of the shank along the X-axis (anterior-posterior direction), the Y-axis (vertical direction), and the pitch rotation (θ) . The shank trajectories for 20 straight walk (3-DOF) cycles were recorded for each subject. For each subject, an average gait cycle trajectory across the 20 recorded trajectories was estimated. Figure 1(a) shows the average gait cycle trajectory for a representative subject. Additionally, the force plate recorded the ground reaction forces on the feet and the moments around the subjects' ankles. The forces and moments were translated to the shank coordinate frame, using the shank and foot center of rotations as described in Ref. [5]. The translated force and torque for the representative subject are shown in Fig. 1(b).

Based on the observed 3-DOF gait trajectories in Fig. 1, a 3-DOF 3-RPR parallel manipulator is proposed to emulate recorded gait trajectories using a lower limb prosthesis. The range of X-axis translation (anterior-posterior direction) shown in Fig. 1(a) (dashed red line) is significantly large, which would affect the size of the 3-RPR parallel manipulator adversely. To remedy this issue, a prismatic joint q_4 is added to the emulator design to extend its workspace [Fig. 2(a)]. The prismatic joint q_4 can be realized as a wheeled mobile platform or a belt and slider mechanism [18] to prolong the translation along the X-axis. By adding the joint q_4 , it is possible to perform the substantial X-axis translation of a gait cycle, through hybrid motion control. For simplicity, joint q_4 follows a constant velocity of the average speed of the anterior translation of the shank. MATLAB's polyfit function is used to split the X-translation of the gait data [Fig. 1(a)] into two components: a constant velocity

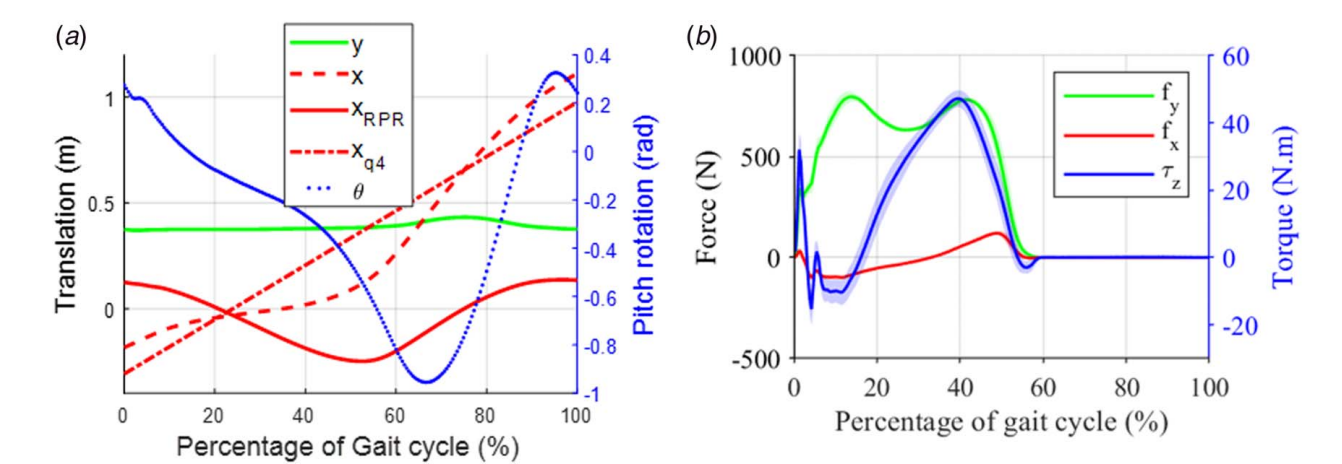


Fig. 1 Average and standard deviation of the (a) kinematics of a complete gait cycle consists of the x and y translations and pitch rotation, where the overall anterior–posterior translation of the shank across a gait cycle (dashed line) will be divided into x-axis translation required by 3-RPR (solid line) and q_4 translation (dotted line) and (b) dynamics of the human shank in the sagittal plane during the complete gait cycle for a representative subject. The gait cycle lasted 0.98 s.

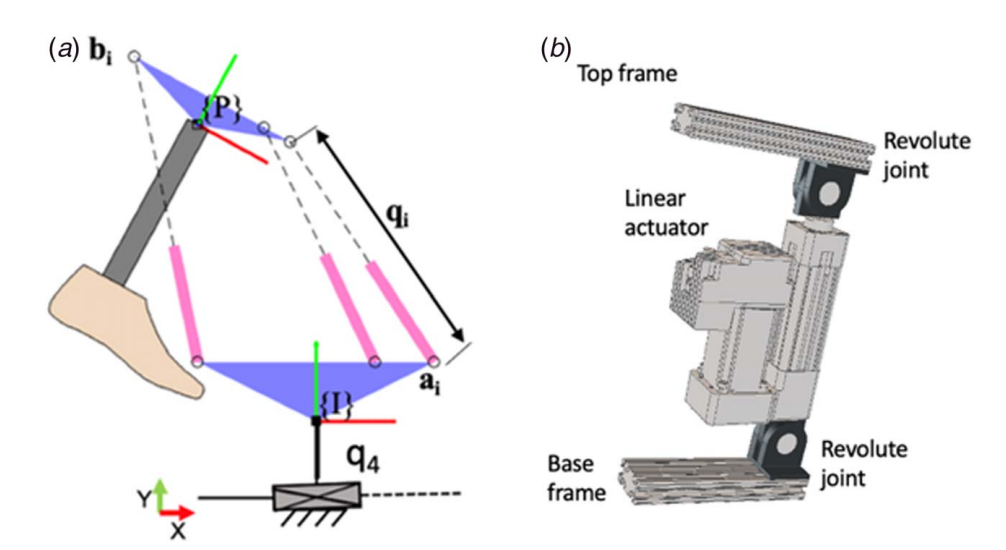


Fig. 2 (a) Proposed 3-RPR parallel manipulator to emulate the gait trajectory of the shank in the sagittal plane. The three kinematic chains of the manipulator lie in different planes to avoid self-collision. (a) Design parameters are defined relative to a base frame and (b) kinematic chains, q_i (i=1,2,3) and moving top frame/end-effector. The prismatic joint q4 extends the translation capability of the 3-RPR manipulator. (b) Rendered CAD model of the kinematic chain

(non-accelerated) and an accelerated component. It can be seen that q_4 limits the required X translation by the 3-RPR to a range of $-0.25 \,\mathrm{m}$ to $0.15 \,\mathrm{m}$, rather than to $-0.2 \,\mathrm{m}$ to $1.1 \,\mathrm{m}$. The final desired trajectory of the onboard 3-RPR parallel manipulator is shown in Fig. 1(*a*).

3 Design Parameters of 3-Revolute, Prismatic, Revolute Parallel Manipulator

The 3-RPR parallel manipulator has three actuated kinematic chains, as shown in Fig. 2(a). Each of the three kinematic chains consists of two passive revolute joints with an active prismatic joint in between. The top frame [Fig. 2(b)] acts as the manipulator's end-effector, which is rigidly attached to the shank. The kinematic chains [Fig. 2(b)] can be contained in any vertical plane as long as this plane is parallel to the sagittal plane, making the 3-RPR a planar parallel mechanism.

All coordinates of the 3-RPR parallel manipulator are defined in the sagittal plane (X and Y axes). Three revolute joints are connected to the bottom frame at a_i , defined relative to the frame {I}, q_i represents the length of the actuated kinematic chain (i). At the other end, the three revolute joints are connected to the top frame at (b_i) , defined relative to the frame {P}. The desired trajectory of

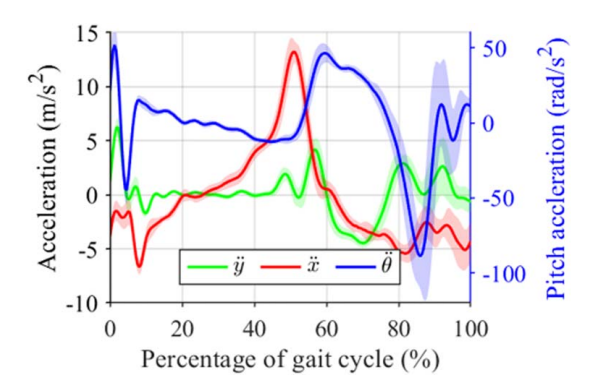


Fig. 3 The acceleration of the end-effector during mimicking the gait cycle of a representative subject

the end-effector (X) is shown in Fig. 1(a). Since a_i , b_i and X are known vectors, the inverse kinematics of the system can determine q_i . X represents X-axis (X_1) , the Y-axis (X_2) , and the pitch rotation (X_2, θ) .

$$\mathbf{a}_{i}, \mathbf{b}_{i} \in \mathbb{R}^{2} \text{ and } \mathbf{X} \in SE(3),$$

$$q_{i} = \left\| \begin{bmatrix} X_{1} \\ X_{2} \end{bmatrix} + R_{z}(X_{3}).\mathbf{b}_{i} - \mathbf{a}_{i} \right\|$$

$$i = 1, 2, 3$$
(1)

The ground reaction force applied to the 3-RPR starts at heel strike (0% gait cycle), as shown in Fig. 1(b). The end-effector is also subjected to inertial forces caused by the desired acceleration of the end-effector (\ddot{X}) through the trajectory (Fig. 3).

The inertial force and torque caused by the inertia of the end-effector is calculated using the mass of the end-effector (M) and the moment of inertia (I) around its center of mass.

$$\boldsymbol{F_D} = \begin{bmatrix} M & 0 & 0 \\ 0 & M & 0 \\ 0 & 0 & I \end{bmatrix} \ddot{\boldsymbol{X}} - \begin{bmatrix} 0 \\ -Mg \\ 0 \end{bmatrix}$$
 (2)

The total end-effector force and torque, F_T , is the sum of the inertial gravitational forces (F_D) and ground reaction force and torque (F_X) , where F_X , F_D and $F_T \in \mathbb{R}^3$.

$$F_T = -F_X + F_D \tag{3}$$

4 Optimizing the Design of 3-Revolute, Prismatic, Revolute Parallel Manipulator

The actuated prismatic joints q_1 , q_2 , q_3 , are associated with the displacement of the linear actuators. The required actuator capabilities (maximum force, velocity, and stroke) are needed to be determined to select a suitable set of linear actuators for manufacturing the designed gait emulator. The desired trajectory (X), the expected end-effector force (F_T) , and expected end-effector velocity (X) are used to estimate the performance requirements of the linear actuators. Coriolis force was omitted in this inverse dynamic calculation since the ground reaction force (F_X) is the major contributor to the force requirements. Actuator requirements include the required

actuator thrust force, F_q , the required actuator velocity, V_q , and the required stroke of the linear actuators, q_i . Human data orientated mechanical design of the 3-RPR parallel manipulator ensure the manipulator's ability in closely following the desired input trajectory. The proposed optimization scheme can be expanded to any input trajectory, to find the optimal design of a proposed parallel manipulator. Optimal design will reduce errors caused by singularity configurations of parallel manipulators [21].

The Jacobian matrix of the mechanism allows the conversion from end-effector space (**X**) to joint space (**q**). Thus, provided the total end-effector force and torque (F_T), one can use the J matrix to convert F_T to F_q , where F_q is a vector that represents the required joint forces to produce the desired end-effector forces, F_T . V_q is computed through the J matrix as well.

The Jacobian matrix H is defined as

$$H = J(q, X) = \frac{\partial q}{\partial X} \tag{4}$$

One can write, For F_q , $V_q \in \mathbb{R}^3$,

$$F_T = H.^T F_q \tag{5}$$

$$\boldsymbol{F}_{\boldsymbol{q}} = (\boldsymbol{H}^T)^{-1} \boldsymbol{F}_T \tag{6}$$

$$V_q = H.\dot{X} \tag{7}$$

An ideal 3-RPR parallel manipulator design can achieve the desired trajectory X and end-effector force F_T with minimal displacement (q), forces (F_q) , and velocities (V_q) , from the three linear actuators. The joint space requirements have to be less than the maximum performance capabilities of selected linear actuators. The design parameters of the 3-RPR include six coordinate points: $a_1, a_2, a_3, b_1, b_2, b_3$ [Fig. 2(a)]. Depending on the manipulator design, the requirements in the joint space could change while subjected to the same trajectory (X) and forces (F_T) in the end-effector workspace. Equations (1), (6), and (7) calculate the maximum stroke $(\max_{i,t} |q_i(t)|)$, maximum force $(\max_{i,t} |F_{Qi}(t)|)$,

and maximum velocity ($\max_{i,t} |V_{Qi}(t)|$) through all points of the tra-

jectory for a suggested manipulator design. The maximum values are used in a cost function and weigh independently relative to the maximum performance capabilities of the selected actuators, as shown in Eq. (12). The weights in the cost function are determined using Leaky rectified linear unit (ReLU) [26]. Leaky ReLU transforms the cost function to penalize more on the manipulator design with requirements above a certain threshold. Leaky ReLU allows a small positive gradient (α) when the function is below the threshold. In this case, the threshold value is the maximum actuator requirements, which is specified according to the manufacturer's datasheet, u. u_F , is the actuator's maximum thrust force, u_v , is the actuator's maximum velocity, and u_a , is the actuator's maximum stroke. This nonlinear transformation prioritizes the reduction of all actuators (z) requirements (stroke, force, and velocity) below the three actuator limits (u), simultaneously, rather than minimizing one requirement while allowing another requirement above the actuation limit. This procedure returns the cost value of the selected trajectory, when carried out by a specific 3-RPR parallel manipulator design $(a_1, a_2, a_3, b_1,$ b_2, b_3).

$$\alpha = 0.1$$

$$f(z, u) = \begin{cases}
\frac{(z - u)}{u}, & z > u \\
\alpha \frac{(z - u)}{u}, & z \le u
\end{cases}$$
(8)

Table 1 Fmincon's search boundaries for each design parameter

Parameter	Lower boundary (m)	Upper boundary (m)
a_1	$[-1.5, 0.1]^{T}$	$[2.5, 0.2]^{T}$
a_2	$[-1.8, 0.0]^{\mathrm{T}}$	$[2.2, 0.3]^{\mathrm{T}}$
\boldsymbol{a}_3	$[-2.5, -0.1]^{\mathrm{T}}$	$[-1.5, 0.2]^{\mathrm{T}}$
\boldsymbol{b}_1	$\begin{bmatrix} -2.2, 0.0 \end{bmatrix}^{\mathrm{T}}$ $\begin{bmatrix} -2.0, 0.0 \end{bmatrix}^{\mathrm{T}}$	$[-1.8, 2.0]_{m}^{T}$
$oldsymbol{b}_2 \\ oldsymbol{b}_3$	$[-2.0, 0.0]^{\mathrm{T}}_{-}$	$[2.0, 2.0]^{T}$
\boldsymbol{b}_3	$[-1.8, 0.0]^{\mathrm{T}}$	$[2.2, 2.0]^{\mathrm{T}}$

$$W_{F} = f\left(\max_{i,t} |F_{Qi}(t)|, u_{F}\right) \tag{9}$$

$$W_V = f\left(\max_{i,t} |V_{Qi}(t)|, u_v\right)$$
 (10)

$$W_D = f\left(\max_{i,t} |q_i(t)|, u_q\right)$$
(11)

$$cost = \underset{a_1, a_2, a_3, b_1, b_2, b_3}{argmin} (W_F + W_V + W_D)$$
 (12)

MATLAB's *fmincon* is used to minimize the cost function [27]. *Fmincon* was set to use sequential quadratic programming to find the cost function value using the design parameters of Eq. (12). *Fmincon's* search boundaries are limited to the size specifications of the 3-RPR parallel manipulator and are shown in Table 1.

A general 3-RPR parallel manipulator design should be optimal in the sense that it reduces the requirements of the actuators for a large pool of subjects. As a first step, we recorded the gait trajectories of the six subjects for our case study. Twenty gait trajectories were recorded for each subject, and an average trajectory (\bar{X}_i) was computed for each subject. For each subject, the average trajectory is concatenated ten times, with standard deviation (σ_i) added as shown in Eq. (13). A data set is created of sixty noisy trajectories (X_n) (due to added standard deviation). This data set is representative of all gait trajectories generated by the six participating subjects. The general optimal design for all trajectories is shown in Fig. 4. In future, optimization scheme will be expanded to use gait kinematics data from amputee subjects using a powered prosthesis.

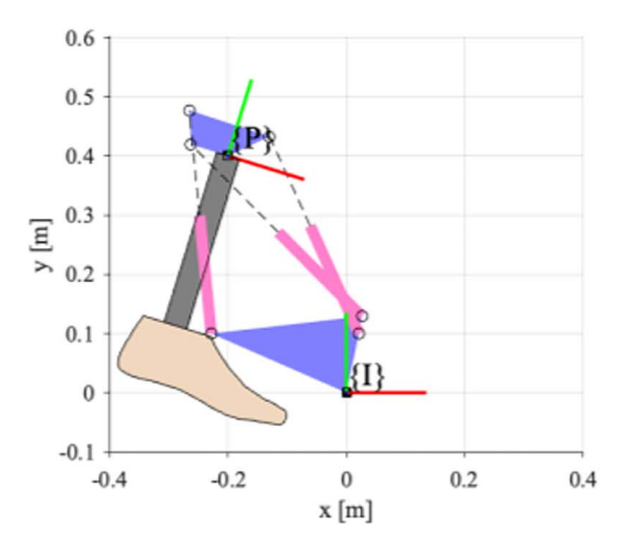
$$X_n = 10 \cdot \bar{X}_i \pm 3\sigma_i \cdot rand(-1,1) \tag{13}$$

where $i = 1, 2, \dots, 6, \bar{X}, \sigma \in \mathbb{R}^3$.

5 Singularity and Workspace Analysis

Singularity configurations can cause significant error in the end-effector's ability to reach the desired position. The Jacobian matrix was analyzed to identify type II singularity configurations of the 3-RPR parallel manipulator general design shown in Fig. 4 [21]. The Jacobian matrix [Eq. (4)] loses its rank when a type II singularity occurs, which causes the determinant of the Jacobian to be zero. However, it is also essential to determine the points in space where the parallel manipulators are close to singularity configurations [28]. A threshold is set to identify singularity points and points close to singularity configurations in the trajectory. No trajectory points (*X*) had a Jacobian matrix determinant (absolute) lower than or equal to 0.05 [19]. The workspace of the designed 3-RPR parallel manipulator was constrained using the maximum stroke





3-RPR Parallel manipulator geometry:

 $\begin{aligned} a_1 &= [0.0212, 0.1000]^T \\ a_2 &= [-0.2283, 0.1000]^T \\ a_3 &= [0.0259, 0.1292]^T \\ b_1 &= [0.0574, 0.0523]^T \\ b_2 &= [-0.0853, 0.0544]^T \\ b_3 &= [-0.0651, 0]^T \end{aligned}$

Actuator Requirements :

Max Force =1,521 N

Max Velocity =1.2592 m/s

Max Stroke = 0.2827 m

Fig. 4 Optimal manipulator design to meet all subjects' requirements. Kinematic chains 1 and 2 lie in the same plane, and third kinematic chain lies in a plane offset 0.4 m from the other kinematic chains.

length of the selected linear actuators, and results are shown in Fig. 5(a).

6 Position Control of the End-Effector

For the designed 3-RPR parallel manipulator, a combination of two control methods is used to minimize trajectory error while compensating for the external force disturbances. PID control is used to track the desired trajectory, while AFC is used to compensate for the recognized force and torque disturbances on the 3-RPR parallel manipulator. We used the gradient descent technique to numerically solve the forward kinematics of the manipulator that was used in the control loop.

A PID controller is used to correct for the error (e) between the desired trajectory (X) and the generated trajectory of the

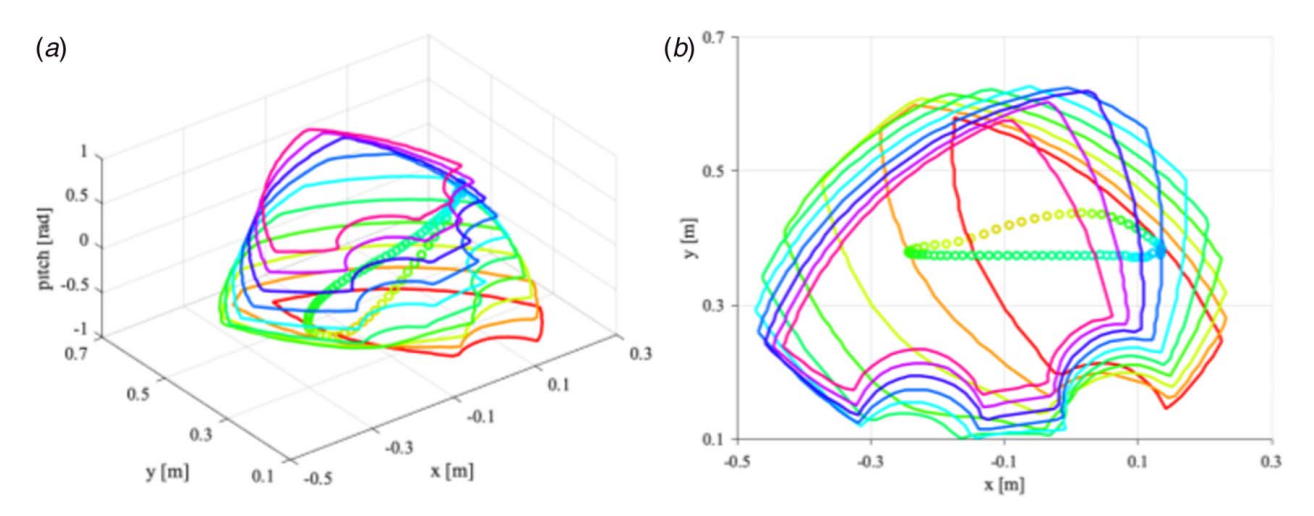


Fig. 5 (a) The workspace of the 3-RPR parallel manipulator in solid lines and the gait trajectory in circular markers. To facilitate visualization, the color is sorted by the pitch value, where consecutive lines represent 0.1 rad increments, ranging from -1.0 to 1. (b) Top view of defined workspace.

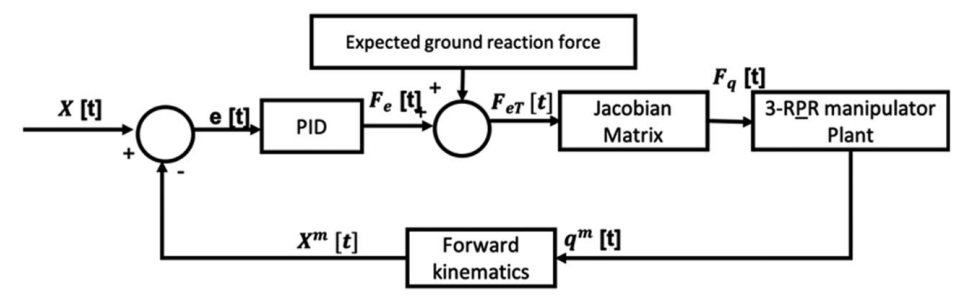


Fig. 6 PID + AFC control of the 3-RPR parallel manipulator

Gain	Xe (N/m)	Ye (N/m)	$\theta_e(\text{N/rad})$
K_P	21,000	25,000	2700
K_I	450	450	100
K_D	280	200	10

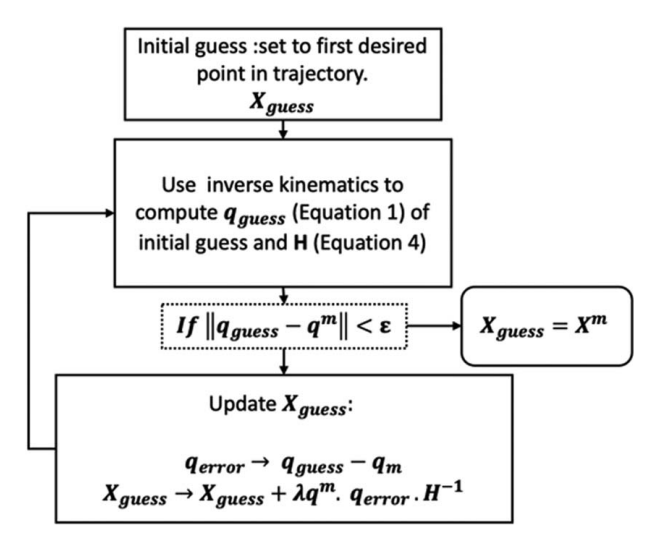
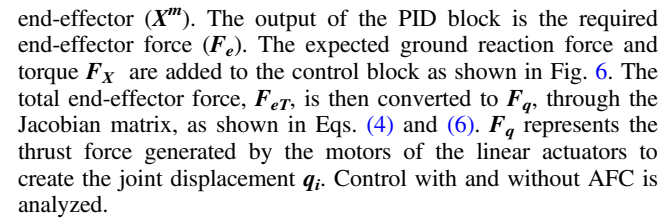


Fig. 7 Flowchart of gradient descent analysis



The overall equation for the PID controller is

$$F_e = K_p \cdot e + K_D \cdot \frac{de}{dt} + K_I \cdot \int e \ dt \tag{14}$$

where X^{ref} , F_e , F_{eT} , F_q , q^m , X^m , $e = [X_e, Y_e, \theta_e]^T \in \mathbb{R}^3$. K_p , K_D , K_I parameters were selected empirically, as shown in Table 2.

7 Case Study of Simulated 3-Revolute, Prismatic, Revolute

MATLAB's Simulink is used to simulate the general 3-RPR parallel manipulator design. The geometry of the plant is shown in Fig. 4. Passive revolute joint blocks simulate the joints in the top and base frames. The prismatic joints (linear actuators) are simulated using actuated prismatic joint blocks. The linear actuators have a maximum thrust force (u_F) of 1521 N, a maximum velocity (u_v) of 1.3 m/s, and a maximum stroke (u_q) of 0.6 m. The simulated prismatic joint blocks are actuated using the computed F_q .

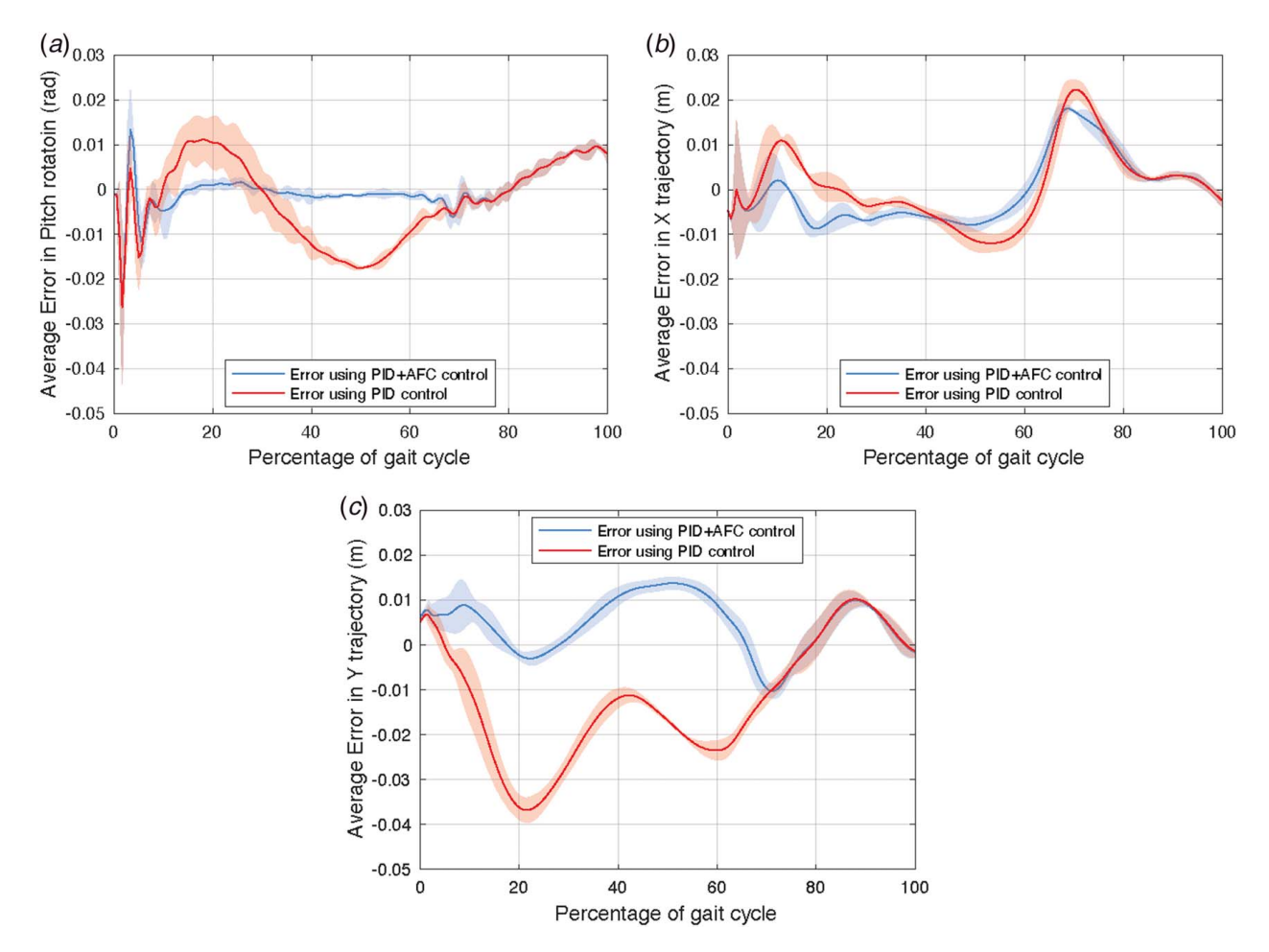


Fig. 8 (a) Average error and standard deviation (2σ) in pitch rotation using PID + AFC and PID control. (b) Average error and standard deviation (2σ) in X-translation using PID + AFC and PID control. (c) Average error and standard deviation (2σ) in Y-translation.

rom http://asmedigitalcollection.asme.org/mechanismsrobotics/article-pdf/15/1/014502/6880708/jmr_15_1_014502.pdf?casa_token=AxY9tgUQSasAAAAA:cwBeFEzF5MkPFHCpFEPn1uKi2XmBzJg6X4rcliCKPpiFDDZZ_R9mSk3M1nhBvtlnervAE8ng by Purdue University at West Lafayette user on

Linear encoders are simulated to measure the actual displacement of prismatic joints (q^m) . The top frame is represented using a plate with a mass (M) of 10 kg and had inertia (I) of 0.1 kg m² around the mass center of the plate. The ground reaction force, F_X is applied to the top frame to mimic the ground reaction force and torque that occurs on the human subject during the gait cycle. A transformation sensor attached to the center of the top plate measures the actual trajectory achieved by the top frame relative to a reference frame. This is aimed to simulate a realistic motion capture system.

For closed-loop analysis, the achieved end-effector position (X^m) is compared to the desired end-effector position (X). Knowing the joint displacement (q^m) and the robot design, one can compute the current end-effector position through solving the forward kinematics problem, which may result in multiple solutions [16]. The forward kinematics block of the 3-RPR parallel manipulator used the measured prismatic displacement (q^m) and the robot design parameters $(a_1, a_2, a_3, b_1, b_2, b_3)$ to compute the achieved trajectory of the end-effector. Gradient descent [29] technique computes a single unique forward kinematics' problem solution as shown in Fig. 7.

$$\mathbf{q}_{\text{guess}}, \ \mathbf{q}^m, \ \mathbf{q}_{\text{error}}, X^m, \ \epsilon \mathbb{R}^3$$

$$\epsilon = 0.0001$$

$$\lambda = 0.085$$

For the design parameters described above, the gradient descent computation took 1 ms per trajectory point using a desktop computer with a 2.2 GHz Quad-Core Intel Core i7 processor. This suggests the suitability of the method for real-time control implementation.

8 Results

To investigate the results of the developed methodology, the performance of the combined PID and AFC controller (PID + AFC) is compared to a PID controller performance. Both control strategies were tested with the control parameters shown in Table 2. The error of each control strategy is the difference between the achieved trajectory of the 3-RPR parallel manipulator (measured using Simulink's transformation sensor) and the desired trajectory (one of the subject's gait cycles). This was repeated for all 20 gait cycles of the representative subject.

Errors between simulation results and actual gait trajectories are calculated. Errors across the 20 cycles are averaged and shown in Fig. 8. The standard deviation (2σ) is also calculated, where the shaded regions represent 95% of the possible error when replicating different trajectories of the subject. The maximum error in the pitch rotation occurs during the swing phase at approximately 60-65% of the gait cycle (depending on the gait speed). This is due to the swing phase requiring significant pitch rotation in a short duration (0.52 s). Both controllers had the same error in regenerating the desired peak pitch rotation; however, PID + AFC control had less error during the stance phase. PID + AFC control produces higher error than PID control alone at certain points due to differences between the expected (average) and actual ground reaction force and torque.

PID + AFC and PID control had the equivalent performance in reducing errors in the X-translation of the gait cycle, because force disturbance in the posterior direction is smaller. Furthermore, PID + AFC had a lower maximum error than PID control by 22%. The maximum ground reaction force in the Y-axis occurs at 0–20% of the gait cycle due to the heel strike [Fig. 1(b)]. As expected, the heel strike causes substantial error in the 3-RPR parallel manipulator's achieved trajectory. PID + AFC had five times lower error compared to the PID control. The reason is that the AFC control

allows the 3-RPR parallel manipulator to be more robust in reducing the error caused by the ground reaction force disturbance.

9 Conclusion and Discussion

A testing platform that can reliably and repetitively replicate realistic gait cycles can be beneficial to the iterative process of design and control of lower extremity robotic prostheses. There are many steps during testing of prostheses, such as fine-tuning controller gains, estimating error in achieving desired ankle impedance [5], testing high-level controllers such as locomotion mode, and user intent control of the prosthesis. These studies would require an extensive data set of gait cycles. The significance of this work includes the ability to test lower limb prosthetic features on instrumented walkways without the need for a human subject.

This paper studied a novel mobile 3-RPR parallel manipulator capable of the trajectory of the human shank during the gait cycle for testing of ankle-foot prostheses. The proposed mechanism used a hybrid motion control, where the forward translation capability was extended by the incorporation of a moving base capable of translating along the posterior-anterior direction during a gait cycle. The designed 3-RPR parallel manipulator was optimized to match the performance capabilities of commercially available linear actuators. The workspace of the designed 3-RPR parallel manipulator was studied to make sure the desired end-effector trajectory resides within its workspace. Gradient descent optimization technique was used to determine a unique solution for the forward kinematics problem of the 3-RPR parallel manipulator. PID control and PID + AFC were implemented to simulate the closed-loop performance of the system. The results concluded that a 3-RPR parallel manipulator using PID+AFC control strategy achieved the desired end-effector trajectory with less error than a manipulator using only traditional PID control.

In future work, we aim to assemble the proposed 3-DOF parallel manipulator and apply the proposed control strategy using a ROS environment. The manipulator will be run on an instrumented walkaway and synchronized with a vibrating platform to estimate the time-varying impedance of prosthetic ankles [6]. Furthermore, we aim to extend the presented method to the design of a three-dimensional parallel manipulator to include turning maneuvers that would generate 6-DOF trajectories for evaluation of prostheses during gait in arbitrary directions.

Funding Data

This research was supported by the National Science Foundation (NSF), Grant Number 1921046.

Conflict of Interest

There are no conflicts of interest.

Data Availability Statement

The datasets generated and supporting the findings of this article are obtainable from the corresponding author upon reasonable request. The data and information that support the findings of this article are freely available.²

References

[1] Richter, H., Simon, D., Smith, W. A., and Samorezov, S., 2015, "Dynamic Modeling, Parameter Estimation and Control of a Leg Prosthesis Test Robot," Appl. Math. Model., 39(2), pp. 559–573.

 $^{^2} https://drive.google.com/file/d/1TRiFfkQLhEHT69swyBF2XEbjEPJNRBF8/view?usp=sharing$

g

- [2] Ficanha, E., Dallali, H., and Rastgaar, M., "Gait Emulator for Evaluation of a Powered Ankle-Foot Prosthesis," ASME 2017 Dynamic Systems and Control Conference, Tysons Corner, VA, Oct. 11–13.
- [3] Rouse, E. J., Hargrove, L. J., Peshkin, M. A., and Kuiken, T. A., "Design and Validation of a Platform Robot for Determination of Ankle Impedance During Ambulation," 2011 Annual International Conference of the IEEE Engineering in Medicine and Biology Society, Boston, MA, Aug. 30–Sept. 3, pp. 8179–8182.
- [4] Nalam, V., and Lee, H., 2019, "Development of a Two-Axis Robotic Platform for the Characterization of Two-Dimensional Ankle Mechanics," IEEE ASME Trans. Mechatron., 24(2), pp. 459–470.
- [5] Ficanha, E. M., Ribeiro, G. A., and Rastgaar, M., 2016, "Design and Evaluation of a 2-DOF Instrumented Platform for Estimation of the Ankle Mechanical Impedance in the Sagittal and Frontal Planes," IEEE ASME Trans. Mechatron., 21(5), pp. 2531–2542.
- [6] Ficanha, E., Ribeiro, G. A., and Rastgaar, M., "Validation of a 2-DOF Instrumented Vibrating Platform for Estimation of the Time-Varying Impedance of the Ankle," ASME Dynamic Systems and Control Conference (DSCC), Minneapolis, MN, July 6–8.
- [7] Dallali, H., Knop, L., Castelino, L., Ficanha, E., and Rastgaar, M., 2017, "Estimating the Multivariable Human Ankle Impedance in Dorsi-Plantarflexion and Inversion-Eversion Directions Using EMG Signals and Artificial Neural Networks," Int. J. Intell. Robot. Appl., 1(1), pp. 19–31.
- [8] Collins, S. H., Kim, M., Chen, T., and Chen, T., "An Ankle-Foot Prosthesis Emulator with Control of Plantarflexion and Inversion-Eversion Torque," 2015 IEEE International Conference on Robotics and Automation (ICRA), Seattle, WA, May 26–30, pp. 1210–1216.
- [9] Chiu, V. L., Voloshina, A. S., and Collins, S. H., 2020, "An Ankle-Foot Prosthesis Emulator Capable of Modulating Center of Pressure," IEEE Trans. Biomed. Eng., 67(1), pp. 166–176.
- [10] Yul Shin, S., Deshpande, A. D., and Sulzer, J., 2018, "Design of a Single Degree-of-Freedom, Adaptable Electromechanical Gait Trainer for People With Neurological Injury," J. Mech. Robot., 10(4), p. 044503.
- [11] Lee, J. Y., 2017, A Lower-Limb Exoskeleton Emulator to be Employed in Estimation of HIP Impedance in Normal Gait, 2017 – Mines Theses & Dissertations, p. 80.
- [12] Hedrick, E. A., Malcolm, P., Wilken, J. M., and Takahashi, K. Z., 2019, "The Effects of Ankle Stiffness on Mechanics and Energetics of Walking With Added Loads: A Prosthetic Emulator Study," J. NeuroEng. Rehabil., 16(1), p. 148.
- [13] Alamdari, A., Haghighi, R., and Krovi, V., 2018, "Stiffness Modulation in an Elastic Articulated-Cable Leg-Orthosis Emulator: Theory and Experiment," IEEE Trans. Robot., 34(5), pp. 1266–1279.
- [14] Thatte, N., Shah, T., and Geyer, H., 2019, "Robust and Adaptive Lower Limb Prosthesis Stance Control via Extended Kalman Filter-Based Gait Phase Estimation," IEEE Robot. Autom. Lett., 4(4), pp. 3129–3136.

- [15] Azocar, A. F., Mooney, L. M., Hargrove, L. J., and Rouse, E. J., "Design and Characterization of an Open-Source Robotic Leg Prosthesis," 2018 7th IEEE International Conference on Biomedical Robotics and Biomechatronics (Biorob), Enschede, The Netherlands, Aug. 26–29, pp. 111–118.
- [16] Patel, Y. D., and George, P. M., 2012, "Parallel Manipulators Applications—A Survey," Mod. Mech. Eng., 2(3), pp. 57–64.
- [17] Amirat, Y., Francois, C., Fried, G., Pontnau, J., and Dafaoui, M., 1996, "Design and Control of a new six DOF Parallel Robot: Application to Equestrian Gait Simulation," Mechatronics, 6(2), pp. 227–239.
 [18] Chen, Y., and Wang, W., 2018, "A Robotic Lift Assister: A Smart Companion for
- [18] Chen, Y., and Wang, W., 2018, "A Robotic Lift Assister: A Smart Companion for Heavy Payload Transport and Manipulation in Automotive Assembly," IEEE Robot. Autom. Mag., 25(2), pp. 107–119.
- [19] Lenarčič, J., and Wenger, P., eds., 2008, Advances in Robot Kinematics: Analysis and Design, Springer, New York.
- [20] Gan, D., Dai, J. S., Dias, J., and Seneviratne, L., 2015, "Forward Kinematics Solution Distribution and Analytic Singularity-Free Workspace of Linear-Actuated Symmetrical Spherical Parallel Manipulators," ASME J. Mech. Rob., 7(4), p. 041007.
- [21] Gosselin, C., and Angeles, J., 1990, "Singularity Analysis of Closed-Loop Kinematic Chains," IEEE Trans. Robot. Autom., 6(3), pp. 281–290.
- [22] Joshi, S. A., and Tsai, L.-W., 2002, "Jacobian Analysis of Limited-DOF Parallel Manipulators," ASME J. Mech. Des., 124(2), pp. 254–258.
- [23] Kong, X., and Gosselin, "Forward Displacement Analysis Of A Quadratic Planar Parallel Manipulator: 3-Rpr Parallel Manipulator With Similar Triangular Platforms," ASME 2008 International Design Engineering Technical Conferences & Computers and Information in Engineering Conference, Brooklyn, NY, Aug. 3-6.
- [24] Noshadi, A., Mailah, M., and Zolfagharian, A., "Active Force Control of 3-RRR Planar Parallel Manipulator," 2010, International Conference on Mechanical and Electrical Technology, Singapore, Sept. 10–12, pp. 77–81.
- [25] Honegger, M., Codourey, A., and Burdet, E., 1997, "Adaptive Control of the Hexaglide, a 6 dof Parallel Manipulator," Proceedings of International Conference on Robotics and Automation, Albuquerque, NM, Apr. 25, Vol. 1, pp. 543–548.
- [26] Xu, B., Wang, N., Chen, T., and Li, M., 2015, "Empirical Evaluation of Rectified Activations in Convolutional Network." ArXiv150500853 Cs Stat, Accessed June 29, 2020.
- [27] Byrd, R. H., Gilbert, J. C., and Nocedal, J., 2000, "A Trust Region Method Based on Interior Point Techniques for Nonlinear Programming," Math. Program., 89(1), pp. 149–185.
- [28] Liu, X.-J., Wu, C., and Wang, J., 2012, "A New Approach for Singularity Analysis and Closeness Measurement to Singularities of Parallel Manipulators," ASME J. Mech. Rob., 4(4), p. 041001.
- [29] Shah, 2018, Gradient Descent: Theory [Video]. SAGE Research Methods Video: Data Science, Big Data Analytics, and Digital Methods.